J. Fluid Mech. (1994), *vol.* 277, *pp.* 249–269

The onset of transverse recirculations during flow of gases in horizontal ducts with differentially heated lower walls

By N. K. INGLE AND T. J. MOUNTZIARIS†
Department of Chemical Engineering and Center for Electronic and Electro-optic Materials, State University of New York, Buffalo, NY 14260, USA

(Received 20 October 1993 and in revised form 12 May 1994)

A computational study has been performed to identify the onset of transverse buoyancy-driven recirculations during laminar flow of hydrogen and nitrogen in horizontal ducts with cool upper walls, and lower walls consisting of three sections: a cool upstream section, a heated middle section and a cool downstream section. The motivation for this work stems from the need to identify operating conditions maximizing the thickness uniformity, the interface abruptness and the precursor utilization during growth of thin films and multi-layer structures of semiconductors by metalorganic chemical vapour deposition (MOCVD). A mathematical model describing the flow and heat transfer along the vertical midplane of MOCVD reactors with the above geometry has been developed and computer simulations were performed for a variety of operating conditions using the Galerkin finite-element method. At atmospheric pressure and low inlet velocities, transverse recirculations form near the upstream and downstream edges of the heated section. These can be suppressed either by increasing the inlet velocity of the gas, so that forced convection dominates natural convection, or by decreasing the operating pressure to reduce the effects of buoyancy. The onset of transverse recirculations has been determined for Grashof (Gr) and Reynolds (Re) numbers covering the following ranges: $10^{-3} < Re < 100$ and $1 < Gr < 10^6$, with Gr and Re computed using fluid properties at the inlet conditions. The computations indicate that, for abrupt temperature changes along the lower wall (worst-case scenario), transverse recirculations are always absent if the following criteria are satisfied:

$$(Gr/Re) < 100 \quad \text{for} \quad 10^{-3} < Re \leqslant 4 \quad \text{and} \quad (Gr/Re^2) < 25 \quad \text{for} \quad 4 \leqslant Re < 100.$$

The predicted critical values of Re, which correspond to the onset of transverse recirculations, agree well with reported experimental observations. The above criteria can be used for optimal design and operation of horizontal MOCVD reactors and may also be useful for heat transfer studies in horizontal ducts with differentially heated lower walls.

1. Introduction

The flow of hydrogen and nitrogen in horizontal ducts with cool upper walls and differentially heated lower walls has been studied to identify the onset of transverse buoyancy-driven recirculations. This problem has important implications in the

† Author to whom all the correspondence should be addressed.

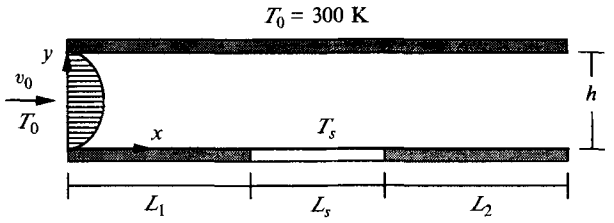

FIGURE 1. Two-dimensional schematic of a horizontal MOCVD reactor showing the vertical and downstream dimensions. The reactor is a horizontal duct with a rectangular cross-section and a differentially heated lower wall. The heated section of the lower wall is called the susceptor.

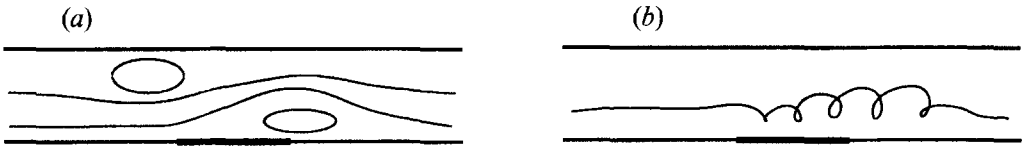

FIGURE 2. Schematic of the two types of buoyancy-driven recirculations formed during mixed convection in horizontal ducts with differentially heated lower walls: (*a*) transverse and (*b*) longitudinal recirculations. The heated area (susceptor) is indicated by the heavy line in the lower wall. The flow is from left to right.

metalorganic chemical vapour deposition (MOCVD) of thin films and multi-layer structures of compound semiconductors, such as GaAs, AlAs, InP and related ternary and quarternary compounds, which form the basis of many advanced electronic and electro-optic devices. Since the development of the MOCVD process in the late 1960s, the underlying flow phenomena have attracted a lot of attention, because they play an important role in determining the quality of the films (Jensen, Einset & Fotiadis 1991).

A very common MOCVD reactor consists of a horizontal duct with a rectangular cross-section and a differentially heated lower wall and is shown schematically in figure 1. The heated section of the lower wall is called the susceptor and this is where the substrate to be coated is placed. During MOCVD of compound semiconductors, a mixture of precursor gases, typically vapours of organometallic liquids diluted in a carrier gas, is passed over the substrate, resulting in the growth of a thin solid film on its surface. The flow is normally laminar and the most common carrier gas has been H_2, but N_2, He and Ar have also been used as carrier gases (Ludowise 1985). In many cases, the upper wall of horizontal reactors is water-cooled to preserve unreacted precursors in the adjacent cold gas stream for film deposition at the downstream part of the substrate. The objective is to increase the thickness uniformity of the films by minimizing the effects of reactant depletion, which takes place along the substrate. However, the resulting unstable thermal stratification may lead to the formation of buoyancy-driven recirculations due to natural convection. These recirculations can be eliminated by increasing the inlet velocity of the gas or by decreasing the operating pressure.

When natural and forced convection coexist, two types of recirculations may arise and are shown schematically in figure 2: (*a*) *transverse recirculations*, whose axes of rotation are horizontal and perpendicular to the direction of bulk flow; (*b*) *longitudinal recirculations*, which produce a helical motion of the fluid in the downstream direction, when superimposed on the forced laminar flow. The axes of rotation of these recirculations are parallel to the direction of bulk flow in this case. Several reported experimental and computational studies have focused on the heat transfer and fluid

mechanics aspects of mixed convection over a horizontal plate, between two horizontal plates or in horizontal ducts. The results of these studies are summarized below.

2. Background

Models of the combined forced and natural convection past an isolated horizontal plate can be traced back to the boundary-layer analyses of Mori (1961) and Sparrow & Minkowycz (1962), who studied the conditions under which buoyancy effects become significant. The full equations of motion and thermal energy describing laminar forced and free convection of a Newtonian Boussinesq fluid past a hot or cold horizontal plate were later solved numerically by Robertson, Seinfeld & Leal (1973). Their solutions for hot plates, i.e. for positive Grashof numbers (*Gr*), indicated an acceleration of the boundary flow near the surface of the plate resulting in increased local skin friction and heat transfer coefficients. The stability of flow between horizontal plates under shear (plane Couette flow) with the lower plate being heated was studied by Deardorff (1965) and by Gallagher & Mercer (1965). They concluded that increasing the Reynolds (*Re*) and Prandtl (*Pr*) numbers will have a stabilizing effect for disturbances in a vertical plane aligned in the direction of mean flow. Shear was found to cause an increase in the critical Rayleigh number (*Ra*) necessary for the development of transverse rolls, but did not have any effect on the critical *Ra* for the development of longitudinal rolls.

Eversteyn *et al.* (1970) were the first to investigate the structure of the flow in horizontal MOCVD reactors, motivated by the need to understand and control the effects of flow phenomena on film quality. They employed flow visualization using light scattering by TiO_2 particles and demonstrated the existence of longitudinal recirculations. Their experiments showed a particle-free zone above the susceptor due to thermophoretic transport of the particles away from the hot region. This artifact led the authors to an erroneous interpretation of the smoke-free zone as a stagnant layer of fluid and to the postulation of a 'stagnant-layer model' of the deposition process. Ban (1978) also observed flow patterns in a horizontal MOCVD reactor using TiO_2 smoke tracing in H_2, He and N_2 for values of (Gr/Re^2) ranging from 0.16 to 12.5 and for susceptor temperatures ranging from 500 °C to 1200 °C. He reported the formation of a fully developed spiral (i.e. a longitudinal recirculation) for $(Gr/Re^2) \geqslant 0.5$, but entrance effects may have played a role in his observations.

Giling (1982) employed the non-intrusive technique of interference holography to visualize flow patterns and temperature profiles during flow of H_2, He, N_2 and Ar in horizontal MOCVD reactors. Thus, he was able to prove that a stagnant layer above the susceptor does not exist. He used both water-cooled and air-cooled upper walls and observed fringe patterns indicating the existence of a cold finger above the susceptor, when the upper wall was air-cooled but hotter than the gas entering the reactor. He also observed entrance effects, which led to undeveloped flow profiles and chaotic patterns in flows of N_2 for either type of wall cooling.

Van de Ven *et al.* (1986) studied experimentally the growth uniformity of GaAs in horizontal MOCVD reactors using H_2 and N_2 as carrier gases. They observed that for *Ra* less than about 700 the flow is dominated by forced convection, whereas for *Ra* larger than about 1700–2800 natural convection becomes important and strong vortex motions are present in the reactor. They also concluded that the ratio (Gr/Re^2) is not a reliable measure to characterize the flow for the range of conditions considered in their study. Moffat & Jensen (1986) performed three-dimensional simulations of flows in a horizontal MOCVD reactor based on a parabolic flow approximation and non-

Boussinesq conditions. They studied the development of longitudinal recirculations and their effects on the thickness uniformity of GaAs films. Their model predicted that the direction of rotation of the longitudinal rolls will depend on the cooling of the sidewalls of the duct. For insulated sidewalls, the fluid will rise along the sidewalls and fall near the centre of the duct. The pattern is reversed for cooled sidewalls.

Chiu & Rosenberger (1987) and Chiu, Ouazzani & Rosenberger (1987) used laser Doppler anemometry to study entrance effects and fully developed longitudinal recirculations during mixed convection of N_2 between two horizontal plates with the lower one being differentially heated. The range of *Ra* and *Re* covered in their study are $1368 < Ra < 8300$ and $15 < Re < 170$ using gas properties computed at the mean temperature. They deduced two entrance lengths from measurements of the velocity profiles: one for the onset of a buoyancy-driven convective instability and another for fully developed mixed convection. They found that the critical *Ra* for transverse recirculations increases as *Re* increases. When transverse recirculations co-existed with longitudinal recirculations, the result was a time-dependent 'snaking' motion of the fluid. It was also shown, both experimentally and by using a mathematical model based on the Boussinesq approximation, that the critical value of *Ra* for the development of longitudinal recirculations is 1708, which is the value obtained from the classical analysis of Rayleigh–Bénard convection (see for example Chandrasekhar 1981).

Visser *et al.* (1989) performed flow visualization experiments using TiO_2 smoke and two-dimensional numerical computations to study transverse recirculations at the leading edge of the susceptor of a horizontal MOCVD reactor with a water-cooled top wall. They varied the susceptor temperature, the flow velocity, the operating pressure, the height of the reactor and the type of carrier gas (H_2 or N_2). The ranges of *Re* and *Gr* covered in their study are $0.1 \leqslant Re \leqslant 10$ and $10 \leqslant Gr \leqslant 10^4$ using gas properties computed at the mean temperature. Their experiments and numerical calculations confirmed that transverse recirculations will occur at the leading edge of the susceptor when the ratio (Gr/Re) exceeds a certain critical value. They also speculated that the ratio (Gr/Re^2) will determine the onset of transverse recirculations for Reynolds numbers higher than about 8.

A two-dimensional computational study by Ouazzani, Chiu & Rosenberger (1988) predicted that buoyancy-driven recirculations in the entrance region of a horizontal MOCVD reactor will result in an increase of the film growth rate at the leading edge of the substrate and a decrease in the downstream region, when compared to a zero-gravity solution. In a subsequent study, Ouazzani & Rosenberger (1990) developed full three-dimensional models, three-dimensional models with parabolic flow approximation, and two-dimensional models of horizontal MOCVD reactors, and compared the predicted growth rates of GaAs with experimental data reported by van de Ven *et al.* (1986). They found that, depending on the aspect ratio and thermal boundary conditions on the sidewalls of the channel, buoyancy-driven three-dimensional flow effects can greatly influence the uniformity of the films, even at subcritical *Ra* (i.e. $Ra < 1708$). Chinoy, Agnello & Ghandhi (1988) combined experimental observations and mathematical modelling to investigate the effects of operating pressure and susceptor slope on the growth uniformity of GaAs in horizontal reactors. Simulations of their experiments indicated that natural-convection effects dominate at near atmospheric pressures and high susceptor slopes.

Field (1989) used a two-dimensional model to study the formation of recirculations in two different horizontal reactors, one with a sloped lower wall before the flat susceptor (Stock & Richter 1986) and another with an upward-tilted susceptor (Field & Ghandhi 1984). By using a flat-susceptor geometry similar to the one described in

figure 1, he developed a simplified analytical expression connecting Gr and Re for the flow profile to be parabolic. The criterion that he proposed is $(Gr/Re) < 24$ and he tested it by simulating flows of H_2 and N_2 in the above reactors. He found that transverse recirculations were always predicted when $(Gr/Re) > 75$. It should be mentioned, however, that the reactors he simulated did not have the geometry shown in figure 1.

The existence of time-dependent flows has been predicted by transient two-dimensional and three-dimensional simulations of flow and heat transfer in horizontal channels with a heated bottom surface and a cooled top surface (Evans & Greif 1989, 1991, 1993). The predicted instability appeared as a combination of transverse travelling waves and longitudinal recirculations in agreement with the observations of Chiu & Rosenberger (1987). The predicted transverse waves disappeared at higher Reynolds numbers and only longitudinal recirculations remained. The presence of this instability was predicted to significantly enhance heat transfer rates, when compared with fully developed flows without instabilities.

Holstein & Fitzjohn (1989) studied the effect of buoyancy forces on the structure of the flow and the growth rate uniformity of InP in cold-wall channel-type MOCVD reactors using two-dimensional simulations of H_2 flows. The operating conditions examined in their study correspond to $1.7 \leqslant Re \leqslant 35$ and $0.042 \leqslant Ra \leqslant 20$ using gas properties computed at the mean temperature. They predicted transverse recirculations in horizontal reactors over both the leading and trailing edges of the susceptor at high (Gr/Re^2) values and predicted that the recirculation at the leading edge of the susceptor is completely eliminated for (Gr/Re^2) smaller than about 7.5. Fotiadis *et al.* (1990) compared the temperature profiles in a horizontal MOCVD reactor obtained by spontaneous Raman scattering to the ones predicted using a two-dimensional flow and heat transfer model for H_2 and N_2 carrier gases. They also observed recirculation cells using smoke tracing experiments, which were successfully reproduced by their model. Fotiadis & Jensen (1990) studied the thermophoresis of solid particles in horizontal MOCVD reactors and found that the predicted particle trajectories are in very good agreement with the smoke tracing experiments of Stock & Richter (1986).

3. Motivation for this study

The elimination of transverse recirculations is essential for growing multi-layer epitaxial structures in horizontal MOCVD reactors with abrupt interfaces between thin films of different semiconductors. These materials are called superlattices or quantum wells and form the basis of several advanced electronic and electro-optic devices, e.g. semiconductor lasers, heterojunction solar cells and high-electron-mobility transistors. The growth of such structures is typically accomplished during a single run by switching from one set of precursor gases to another after a preset period of time. The existence of transverse flow recirculations can have detrimental effects on the abruptness of the interfaces obtained by this technique. If transverse recirculations are present, precursors can be trapped in them and then slowly diffuse to the surface of the film and be incorporated in it, even after they have been turned off and a different set of precursors has been turned on. This delay in the purging of the old precursors results in multi-layer structures with graded interfaces, which are not useful for most devices. To avoid this problem it has become common practice to operate horizontal MOCVD reactors at very high flow rates and/or low pressures to suppress all transverse recirculations and minimize the dispersion of reactants during switching. However, this strategy results in short residence times in the reaction zone and only a small

percentage of the precursors is incorporated in the film. Since these precursors are expensive ultra-pure materials and many of them are also highly toxic (e.g. arsenic compounds), there is at present a great need for improving their utilization during MOCVD of semiconductors.

If the operating conditions corresponding to the onset of transverse recirculations can be determined *a priori*, a lower bound on the permissible flow rates can be established. The flow rates just above the critical ones required for suppressing all transverse recirculations are the appropriate starting conditions for optimization studies. Optimal operating conditions will correspond to the minimum possible flow rates (above the critical ones) producing films with uniform thickness and composition and abrupt interfaces. Detailed models of the mass transfer and kinetics underlying the MOCVD process (e.g. Mountziaris, Kalyanasundaram & Ingle 1993) can be very helpful at this stage, because they can minimize the expensive and time-consuming experimental trial and error. The objective of this work is to solve the first part of the problem by establishing criteria for identifying the onset of transverse recirculations in typical horizontal MOCVD reactors during laminar flow of H_2 or N_2.

4. Modelling equations

The model is based on the fundamental equations of mass continuity, momentum balance and heat balance. It describes the steady flow of an ideal compressible gas with properties that depend on the local temperature and pressure. Two spatial dimensions are considered in this study: a horizontal direction, x, aligned with the macroscopic direction of flow and the vertical direction, y (figure 1). During MOCVD of semiconductors the mixture of precursors in the carrier gas is usually very dilute and the contribution of the heat of reaction to the energy balance is negligible. Furthermore, any expansion or contraction due to reactions is very small as are the heat of mixing and the viscous dissipation. Thus, the flow and heat transfer part of the problem can be very accurately represented by considering only the carrier gas. Finally, the pressure drop in the reactor is typically very small and the inlet pressure p_0 can be used in the computations of the physical properties of the gas.

With the above assumptions the equations are written in dimensionless form using the symbol $\hat{}$ to denote dimensionless quantities. The length L_s of the heated part (susceptor) has been used to scale horizontal lengths, the height h of the duct to scale vertical lengths, the average inlet velocity v_0 to scale velocities, and the product $(\rho_0 v_0^2)$ to scale pressures, where ρ_0 is the density of the gas at inlet temperature $T_0 (= 300\ \mathrm{K})$ and pressure p_0. The dimensionless temperature is defined as $[(T-T_0)/(T_s-T_0)]$, where T_s is the susceptor temperature. All physical and transport properties of the gas are scaled with their corresponding values at temperature T_0 and pressure p_0. The ranges of the parameter values covered in this study are shown in table 1.

The dimensionless modelling equations are

continuity:
$$\alpha\frac{\partial}{\partial\hat{x}}(\hat{\rho}\hat{v}_x)+\frac{\partial}{\partial\hat{y}}(\hat{\rho}\hat{v}_y)=0, \tag{1}$$

x-momentum balance:
$$\hat{\rho}\left(\alpha\hat{v}_x\frac{\partial\hat{v}_x}{\partial\hat{x}}+\hat{v}_y\frac{\partial\hat{v}_x}{\partial\hat{y}}\right)=-\alpha\frac{\partial\hat{p}}{\partial\hat{x}}+\frac{1}{Re}\left\langle\alpha\frac{\partial}{\partial\hat{x}}\left\{\hat{\mu}\left[2\alpha\frac{\partial\hat{v}_x}{\partial\hat{x}}-\frac{2}{3}\left(\alpha\frac{\partial\hat{v}_x}{\partial\hat{x}}+\frac{\partial\hat{v}_y}{\partial\hat{y}}\right)\right]\right\}\right.$$
$$\left.+\frac{\partial}{\partial\hat{y}}\left[\hat{\mu}\left(\frac{\partial\hat{v}_x}{\partial\hat{y}}+\alpha\frac{\partial\hat{v}_y}{\partial\hat{x}}\right)\right]\right\rangle, \tag{2}$$

Type of gas	H_2 or N_2
Height of duct, h	1–5 cm
Susceptor length, L_s	5–15 cm
Entrance length, L_1	15–20 cm*
Exit length, L_2	25–30 cm*
Operating pressure, p_0	0.1–1.0 atm
Susceptor temperature, T_s	320–1300 K
Temperature of upper wall, T_0	300 K
Inlet temperature, T_0	300 K
Reynolds number, Re	$10^{-3} < Re < 100$
Grashof number, Gr	$1 < Gr < 10^6$
Temperature ratio $(T_s - T_0)/T_0$	0.067–3.33

(* Varied to eliminate end effects.)

TABLE 1. Ranges of operating conditions covered in this study

Gas	Thermal conductivity (k) (cal cm^{-1} s^{-1} K^{-1})	Specific heat (c_p) (cal g^{-1} K^{-1})	Viscosity (μ) (cP)
H_2	$1.779\times10^{-4}+9.03\times10^{-7}T(\mathrm{K})$	$3.284+4.02\times10^{-4}T(\mathrm{K})$	$0.0085\times[T(\mathrm{K})/273.15]^{0.65}$
N_2	$2.600\times10^{-5}+1.30\times10^{-7}T(\mathrm{K})$	$0.232+3.57\times10^{-5}T(\mathrm{K})$	$0.0180\times[T(\mathrm{K})/273.15]^{0.63}$

TABLE 2. Temperature dependence of the thermal conductivity, specific heat and viscosity of the two carrier gases used in this study

y-momentum balance:

$$\hat{\rho}\left(\alpha\hat{v}_x\frac{\partial\hat{v}_y}{\partial\hat{x}}+\hat{v}_y\frac{\partial\hat{v}_y}{\partial\hat{y}}\right)=-\frac{\partial\hat{p}}{\partial\hat{y}}+\frac{1}{Re}\left\langle\frac{\partial}{\partial\hat{y}}\left\{\hat{\mu}\left[2\frac{\partial\hat{v}_y}{\partial\hat{y}}-\frac{2}{3}\left(\alpha\frac{\partial\hat{v}_x}{\partial\hat{x}}+\frac{\partial\hat{v}_y}{\partial\hat{y}}\right)\right]\right\}+\alpha\frac{\partial}{\partial\hat{x}}\left[\hat{\mu}\left(\frac{\partial\hat{v}_x}{\partial\hat{y}}+\alpha\frac{\partial\hat{v}_y}{\partial\hat{x}}\right)\right]\right\rangle-\frac{1}{Fr}\hat{\rho}, \quad (3)$$

thermal energy balance:

$$\hat{\rho}\hat{c}_p\left(\alpha\hat{v}_x\frac{\partial\hat{T}}{\partial\hat{x}}+\hat{v}_y\frac{\partial\hat{T}}{\partial\hat{y}}\right)=\frac{1}{Pe}\left[\alpha^2\frac{\partial}{\partial\hat{x}}\left(\hat{k}\frac{\partial\hat{T}}{\partial\hat{x}}\right)+\frac{\partial}{\partial\hat{y}}\left(\hat{k}\frac{\partial\hat{T}}{\partial\hat{y}}\right)\right]. \quad (4)$$

The local density of the gas, ρ, is connected to the pressure and temperature by using the ideal gas law, $\rho = p_0 M/RT$, where M is the molecular weight of the gas and R is the ideal gas constant.

In the above equations v_x and v_y are the x- and y-components of the velocity of the gas, μ is the viscosity of the gas, c_p is the specific heat of the gas at constant pressure, T its temperature and k its thermal conductivity. The functions used to describe the temperature dependence of k, c_p and μ for the two carrier gases have been obtained by fitting data reported in Perry & Chilton (1974) and are listed in table 2.

The following dimensionless numbers appear in the modelling equations: Aspect ratio: $\alpha = h/L_s$, Reynolds number: $Re = (hv_0\rho_0)/\mu_0$, Froude number: $Fr = v_0^2/(gh)$, where g is the gravitational acceleration, Péclet number: $Pe = (hv_0\rho_0 c_{p0})/k_0$.

If the Boussinesq approximation is applied, the dimensionless quantity (Gr/Re^2) will appear as a factor in the buoyancy term of the y-momentum equation (Holstein & Fitzjohn 1989). Although this approximation was not employed in our model, we have chosen to use the Grashof number in the presentation of our results, because it has

been traditionally used in the analysis of natural- and mixed-convection problems. Furthermore, reported experimental data on return flows in horizontal MOCVD reactors have been correlated using Gr and Re (Visser *et al.* 1989). The Grashof number used in the present study was defined as $Gr = [g\rho_0^2 h^3 \beta_0 (T_s - T_0)]/\mu_0^2$, where β_0 is the coefficient of volume expansion equal to $(1/T_0)$ for ideal gases.

Since Fr is equal to $(Re^2/Gr)\,R_T$, where R_T is the temperature ratio $(T_s - T_0)/T_0$, the dimensionless groups of the problem are Gr, Re, R_T, Pe and α. The scaled properties of the gas also appear as parameters in the model. Notice, however, that Gr is proportional to R_T for ideal gases and Pe, which is equal to $Re\,Pr$, is nearly proportional to Re because the Prandtl number $(Pr = c_{p0}\mu_0/k_0)$ is almost constant and equal to about 0.7 for gases. In this work we have chosen to use Gr, Re and α in the analysis of the results. For low-Re flows, the inertial terms in the momentum equations are negligible and the ratio (Gr/Re) is expected to be the dominant dimensionless quantity arising from the y-momentum balance. On the other hand, for high-Re flows the viscous terms become insignificant, when compared to the inertial and buoyancy terms. In such a case, the ratio (Gr/Re^2) becomes the dominant dimensionless quantity.

The model is completed by using the following boundary conditions.

(i) At the inlet of the reactor, a parabolic velocity profile was assumed in the x-direction with no velocity component in the y-direction and a uniform temperature T_0:

$$\hat{v}_y = 6(\hat{y} - \hat{y}^2), \quad \hat{v}_y = 0, \quad \hat{T} = 0; \quad \hat{x} = 0 \quad \text{and} \quad 0 \leqslant \hat{y} \leqslant 1. \tag{5}$$

(ii) At the upper wall, a no-slip condition was imposed on the velocity and a uniform temperature T_0 was assumed:

$$\hat{v}_x = \hat{v}_y = 0, \quad \hat{T} = 0; \quad \hat{y} = 1 \quad \text{and} \quad 0 \leqslant \hat{x} \leqslant (\hat{L}_1 + 1 + \hat{L}_2). \tag{6}$$

(iii) At the lower wall, a no-slip condition was imposed on the velocity

$$\hat{v}_x = \hat{v}_y = 0; \quad \hat{y} = 0 \quad \text{and} \quad 0 \leqslant \hat{x} \leqslant (\hat{L}_1 + 1 + \hat{L}_2). \tag{7}$$

The temperature profile was determined as follows.

(*a*) *Case A*: Isothermal inlet and outlet regions with temperature of wall $T = T_0$ and a step change in temperature at the edges of the susceptor were assumed.

Inlet and outlet regions:

$$\hat{T} = 0 \quad \text{for} \quad \hat{y} = 0 \quad \text{and} \quad 0 \leqslant \hat{x} \leqslant \hat{L}_1 \quad \text{or} \quad (\hat{L}_1 + 1) < \hat{x} \leqslant (\hat{L}_1 + 1 + \hat{L}_2). \tag{8a}$$

Susceptor:

$$\hat{T} = 1 \quad \text{for} \quad \hat{y} = 0 \quad \text{and} \quad \hat{L}_1 \leqslant \hat{x} \leqslant (\hat{L}_1 + 1). \tag{8b}$$

(*b*) *Case B*: Conduction of heat in the lower wall was taken into account.

Inlet and outlet regions:

$$\alpha^2 \frac{\partial^2 \hat{T}}{\partial \hat{x}^2} + \frac{\partial^2 \hat{T}}{\partial \hat{y}^2} = 0 \quad \text{for} \quad -\hat{d} \leqslant \hat{y} \leqslant 0 \quad \text{and} \quad 0 \leqslant \hat{x} \leqslant \hat{L}_1$$
$$\text{or} \quad (\hat{L}_1 + 1) \leqslant \hat{x} \leqslant (\hat{L}_1 + 1 + \hat{L}_2), \tag{9a}$$

where d is the thickness of the wall, taken to be 2 mm in this study.

The above equation (9*a*) was solved simultaneously with the equations describing flow and heat transfer in the gas using the following boundary conditions:

$$\hat{T} = 0 \quad \text{for} \quad \hat{x} = 0 \quad \text{or} \quad \hat{x} = (\hat{L}_1 + 1 + \hat{L}_2) \quad \text{and} \quad -\hat{d} \leqslant \hat{y} \leqslant 0, \tag{9b}$$

$$\hat{T} = 1 \quad \text{for} \quad \hat{x} = \hat{L}_1 \quad \text{or} \quad \hat{x} = (\hat{L}_1 + 1) \quad \text{and} \quad -\hat{d} \leqslant \hat{y} \leqslant 0, \tag{9c}$$

$$\hat{k} \frac{\partial \hat{T}}{\partial \hat{y}} = \hat{k}_w \frac{\partial \hat{T}}{\partial \hat{y}} \quad \text{for} \quad \hat{y} = 0 \quad \text{and} \quad 0 \leqslant \hat{x} \leqslant \hat{L}_1 \quad \text{and} \quad (\hat{L}_1 + 1) \leqslant \hat{x} \leqslant (\hat{L}_1 + 1 + \hat{L}_2) \tag{9d}$$

and

$$\frac{\partial \hat{T}}{\partial \hat{y}} = Nu\,\hat{T} \quad \text{for} \quad \hat{y} = -\hat{d} \quad \text{and} \quad 0 \leqslant \hat{x} \leqslant \hat{L}_1 \quad \text{or} \quad (\hat{L}_1 + 1) \leqslant \hat{x} \leqslant (\hat{L}_1 + 1 + \hat{L}_2), \tag{9e}$$

where Nu is a Nusselt number here defined as $Nu = (h_w h)/k_w$. The value of the local heat transfer coefficient, h_w, was obtained using correlations for natural convection from horizontal flat plates facing down reported in McCabe, Smith & Harriott (1985). The fluid in contact with the outside surface of the wall was assumed to be air with a temperature far from the wall equal to T_0. The thermal conductivity of the wall, k_w, was assumed to be constant and a value for quartz (0.003 cal s^{-1} cm^{-1} K^{-1}) was used in this study, because many MOCVD reactors are made of quartz.

Susceptor:

$$\hat{T} = 1 \quad \text{for} \quad \hat{y} = 0 \quad \text{and} \quad \hat{L}_1 \leqslant \hat{x} \leqslant (\hat{L}_1 + 1). \tag{9f}$$

(iv) At the exit of the reactor a fully developed flow was assumed with zero y-component of velocity:

$$\frac{\partial \hat{v}_x}{\partial \hat{x}} = \frac{\partial \hat{T}}{\partial \hat{x}} = 0 \quad \text{and} \quad \hat{v}_y = 0 \quad \text{for} \quad \hat{x} = (\hat{L}_1 + 1 + \hat{L}_2) \quad \text{and} \quad 0 \leqslant \hat{y} \leqslant 1. \tag{10}$$

The lengths of the inlet and outlet regions, L_1 and L_2, were adjusted to be long enough so that the boundary conditions imposed at those locations do not distort the velocity and temperature profiles in the reactor. Finally, the reactor pressure was defined at one point at the exit of the reactor.

5. Numerical method

The equations were solved numerically using the Galerkin finite-element method (Strang & Fix 1973). The domain was discretized into rectangular elements. A typical mesh consisted of 20 elements in the vertical direction and 80 in the horizontal direction. A higher concentration of elements was placed near the susceptor to resolve the steep gradients in that region. The optimal number of elements was selected by increasing the resolution until the predicted velocity and temperature profiles did not depend on the number of elements. Biquadratic basis functions were used to approximate velocities and temperature and bilinear basis functions to approximate pressure. The computations were performed on a Cray C90 supercomputer and required about 5 CPU seconds per Newton iteration. A typical run required 3–5 Newton iterations to converge. Continuation techniques using either the temperature of the susceptor or the inlet velocity as parameters were applied to obtain good initial guesses for subsequent runs. The dimensional equations were also solved to fully understand the effects of operating conditions on the onset of transverse recirculations.

6. Results and discussion

An example of computed flow profiles at three different inlet velocities is shown in figure 3 for hydrogen carrier gas and detailed thermal boundary conditions along the entrance and exit regions of the lower wall (Case B, see §4). At low velocities, two

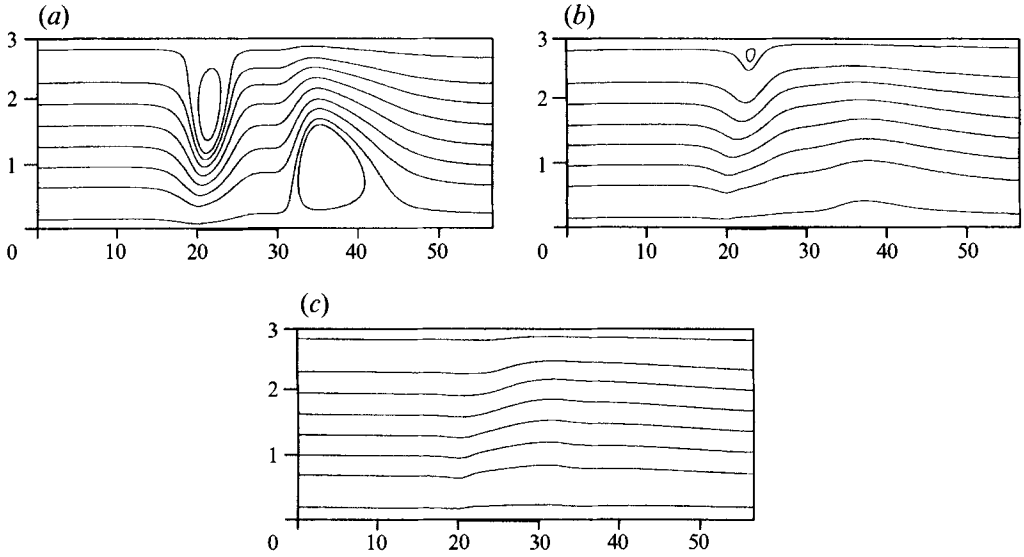

FIGURE 3. Pathlines of hydrogen at different inlet velocities: (*a*) At $v_0 = 4$ cm s^{-1} ($Re = 10.9$) two transverse recirculations are present. (*b*) At $v_0 = 8$ cm s^{-1} ($Re = 21.8$) the downstream recirculation has been suppressed. (*c*) At $v_0 = 12$ cm s^{-1} ($Re = 32.7$) both recirculations have been suppressed. Other conditions: $p_0 = 1$ atm, $T_s = 1000$ K, $Gr = 15300$, $h = 3$ cm, $L_1 = 20$ cm, $L_s = 10$ cm, $L_2 = 25$ cm and $\alpha = 0.3$. The heat conduction in the lower wall has been taken into account (Case B). All dimensions are in cm. The heated part of the lower wall is indicated by the heavy line.

transverse recirculation cells develop in the reactor. The first forms near the upper wall above the upstream edge of the susceptor and rotates in a counterclockwise direction. The second forms near the lower wall beyond the downstream edge of the susceptor and rotates in a clockwise direction. By increasing the inlet velocity from 4 cm s^{-1} to 8 cm s^{-1} the downstream recirculation is completely eliminated and the upstream one shrinks significantly. A further increase of the inlet velocity to 12 cm s^{-1} eliminates the upstream recirculation too. The elimination of the recirculations is due to the domination of the forced convection over the natural convection. In this example the upstream recirculation is more persistent, but the reverse can be true under different operating conditions, which are discussed below.

To understand the evolution of the flow profiles as the inlet velocity is increased, consider the limiting case of zero inlet velocity. Since the lower wall is differentially heated, two buoyancy-driven recirculation cells will typically develop over the edges of the susceptor even at values of Gr below the limit predicted by the Rayleigh–Bénard theory. The gas will be heated and rise over the hot susceptor, come in contact with the cool upper wall and descend in the upstream and downstream regions. If a horizontal flow is superimposed on the buoyancy-driven convection, the upstream roll, which is rotating counterclockwise, will be displaced towards the upper wall and further downstream over the heated region (figure 3*a*). The downstream roll, which is rotating clockwise, will be displaced towards the lower wall and away from the heated region. As the inlet velocity is increased the two rolls will move further downstream, shrink and eventually disappear, the upstream one at a point along the upper wall and the downstream one at a point along the lower wall (figures 3*b*, *c*).

Figure 4 shows the temperature profiles corresponding to the flow profiles of figure 3. The entire length of the upper wall is kept at 300 K, while the temperature of the lower wall is predicted to drop quickly to 300 K away from the hot susceptor. At low

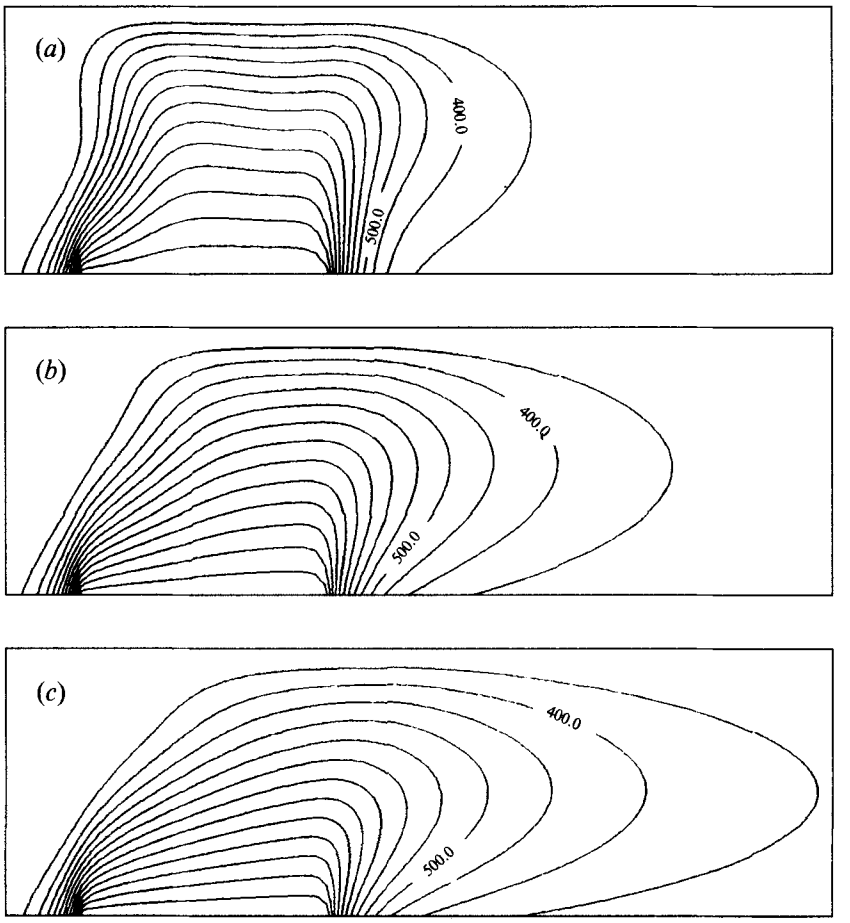

FIGURE 4. Temperature profiles during flow of hydrogen at operating conditions corresponding to figure 3. The isotherms are plotted every 50 K.

and intermediate velocities there is an apparent distortion of the temperature profile by the upstream recirculation (figures 4*a*, *b*). There is also a visible distortion of the temperature profile due to the downstream recirculation at low inlet velocities (figure 4*a*). When both recirculations have been eliminated at the higher inlet velocity, the temperature profile above the upstream part of the susceptor resembles that of a boundary layer over a flat plate (figure 4*c*).

The operating conditions corresponding to the onset of transverse recirculations were identified by searching for the existence of horizontal velocity components pointing in the negative x-direction. First-order continuation was subsequently employed for each recirculation and the inlet velocity was adjusted to force the negative horizontal velocities with the maximum absolute values to zero. By using this technique, the parameter space described in table 1 was searched efficiently and the two critical Reynolds numbers, Re_1 for the onset of the upstream recirculation and Re_2 for the onset of downstream one, were identified for different values of the Grashof number and the aspect ratio.

Figure 5 shows the effects of changing the duct height on Re_1 and Re_2 for a reactor having a 10 cm long susceptor and operating at atmospheric pressure. As the upper wall is moved away from the susceptor, the viscous terms of the equation of motion,

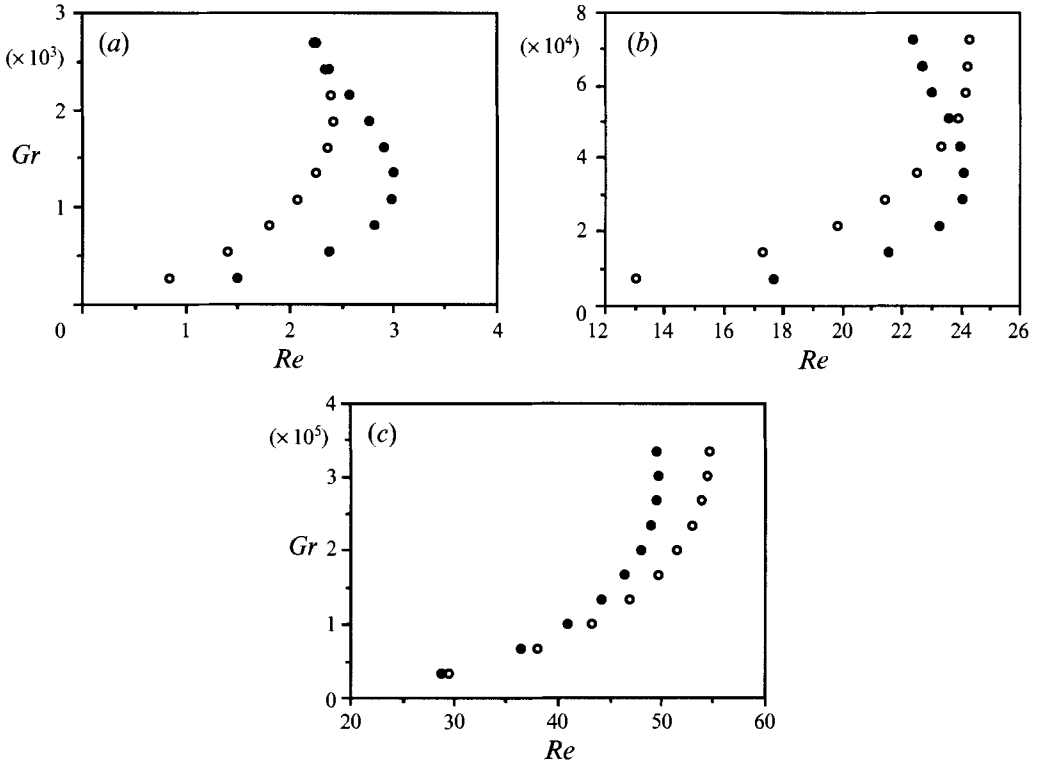

FIGURE 5. The effects of changing the distance between the upper and lower wall on the critical Reynolds numbers for elimination of the upstream (Re_1: ○) and the downstream (Re_2: ●) transverse recirculations during flow of hydrogen at different Grashof numbers. (*a*) h = 1 cm (α = 0.1), (*b*) h = 3 cm (α = 0.3), (*c*) h = 5 cm (α = 0.5). In each case the susceptor temperature has been increased from 400 to 1300 K in steps of 100 K. Other conditions: p_0 = 1 atm, L_s = 10 cm step changes in the temperature of the lower wall (Case A).

which are important in the areas of slow-moving fluid near the walls, play a smaller role in preventing the formation of recirculations. As a result, higher inlet velocities are required to eliminate the recirculations at larger duct heights. This is reflected in the critical *Re* values, which increase faster than h. Another observation is that for small duct heights the downstream recirculation is the most dominant one, but this scenario changes as the reactor height is increased from 1 cm (figure 5*a*) to 3 cm (figure 5*b*) and is completely reversed at 5 cm (figure 5*c*). In the latter case, the upstream recirculation becomes more persistent, because the higher inlet velocities required to reach the critical conditions push it into the region directly above the leading edge of the susceptor. There, the unstable thermal stratification and the expansion of the gas, due to heating from below, tend to sustain it longer compared to the downstream one.

As the susceptor temperature increases (i.e. as *Gr* increases), the predicted Re_2 passes through a maximum and then decreases. High susceptor temperatures lead to increased gas expansion, but the cool upper wall prevents the boundary layer from developing in the vertical direction beyond a certain point. As a result, the gas expands horizontally and the convection in this direction is increased. This effect plays a significant role in eliminating the downstream recirculation by reducing the requirements on the horizontal convection imposed at the inlet. As the reactor height is increased, the maximum in the Re_2 curve appears at higher susceptor temperatures. A similar trend

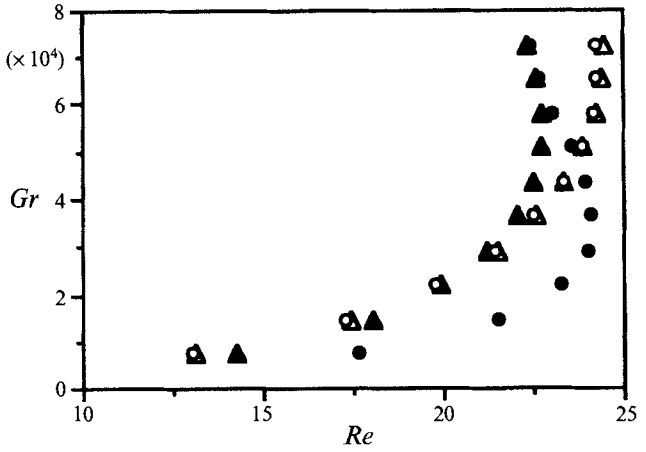

FIGURE 6. The effects of changing the length of the heated susceptor on the critical Reynolds numbers for elimination of transverse recirculations during flow of hydrogen at different Grashof numbers. $L_s = 10$ cm ($\alpha = 0.3$): ○, Re_1; ●, Re_2. $L_s = 5$ cm ($\alpha = 0.6$): △, Re_1; ▲, Re_2. In each case the susceptor temperature has been increased from 400 to 1300 K in steps of 100 K. Other conditions: $p_0 = 1$ atm, $h = 3$ cm and step changes in the temperature at the edges of the heated section (Case A).

is observed in the Re_1 curve of figure 5(*a*) at high susceptor temperatures (i.e. high Gr values). An increase in the gas viscosity in the region of the upstream roll, due to back-diffusion of heat, is probably responsible for this trend. The back-diffusion of heat is more significant at low inlet velocities associated with critical conditions in reactors with small heights.

The effect of decreasing the susceptor length from 10 to 5 cm, while keeping the duct height constant at 3 cm and the pressure at 1 atm, is shown in figure 6. As expected, the length of the susceptor has virtually no effect on the onset of the upstream recirculation. However, it significantly affects the downstream one at low susceptor temperatures (low Gr). This recirculation is found to be more persistent at longer susceptor lengths owing to more efficient heating of the gas. As the temperature of the susceptor (and the value of Gr) increases, the Gr versus Re_2 curves approach each other and collapse into a single curve at a certain temperature. At that point, the temperature profiles over the downstream edge of the susceptor are nearly identical, because in both cases the boundary layers are developed in the vertical direction all the way to the upper wall.

If the susceptor temperature is kept constant and its length is increased, the flow over it will become fully developed beyond a certain point. Any further increase in the susceptor length will not have a significant effect on the onset of the downstream recirculation, if all other operating conditions are kept constant. For the range of operating conditions covered in this study, the susceptor length had very little effect in determining the onset of transverse recirculations beyond the value of 10 cm. It should be mentioned that longer susceptor lengths may be required for obtaining fully developed flow in the presence of longitudinal recirculations (Chiu *et al.* 1987).

As the operating pressure decreases, the effects of buoyancy and inertia become less important and the recirculations can be eliminated at lower inlet velocities and lower Re. Figure 7 shows the effects of changing the operating pressure from 1 atm to 0.5 atm and down to 0.1 atm on the onset of transverse recirculations of hydrogen gas in a reactor with a height of 3 cm and a susceptor length of 10 cm (i.e. with $\alpha = 0.3$). Notice that, as the pressure decreases, the critical Re values decrease by a factor larger than

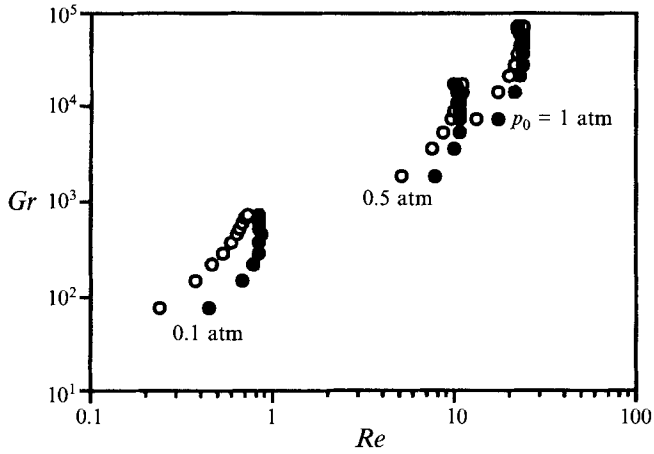

FIGURE 7. The effects of changing the operating pressure from 1 atm to 0.1 atm on the critical Reynolds numbers for elimination of the upstream (Re_1: ○) and the downstream (Re_2: ●) transverse recirculations during flow of hydrogen at different Grashof numbers. In each case the susceptor temperature has been increased from 400 to 1300 K in steps of 100 K. Other conditions: h = 3 cm, L_s = 10 cm and step changes in the temperature at the edges of the heated section (Case A).

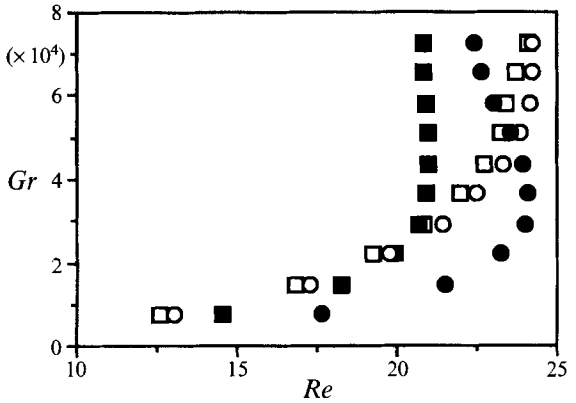

FIGURE 8. The effects of changing the thermal boundary condition along the lower wall on the critical Reynolds numbers for elimination of transverse recirculations during flow of hydrogen at different Grashof numbers. Case A (step changes in temperature at the edges of the heated section): ○, Re_1; ●, Re_2. Case B (heat conduction in lower wall is taken into account): □, Re_1; ■, Re_2. In each case the susceptor temperature has been increased from 400 to 1300 K in steps of 100 K. Other conditions: p_0 = 1 atm, h = 3 cm and L_s = 10 cm.

the one corresponding to the decrease in the operating pressure. This indicates lower critical inlet velocities at low pressures. Furthermore, the upstream recirculation becomes less persistent at low pressures when compared to the downstream one. This trend is similar to the one predicted in figure 5, where an increase in the critical velocity led to a more persistent upstream roll.

Figure 8 shows the effects of changing the thermal boundary conditions along the upstream and downstream sections of the lower wall on Re_1 and Re_2. As expected, the most persistent recirculations are obtained when a step change is imposed on the temperature at the edges of the susceptor (Case A), because this leads to steeper

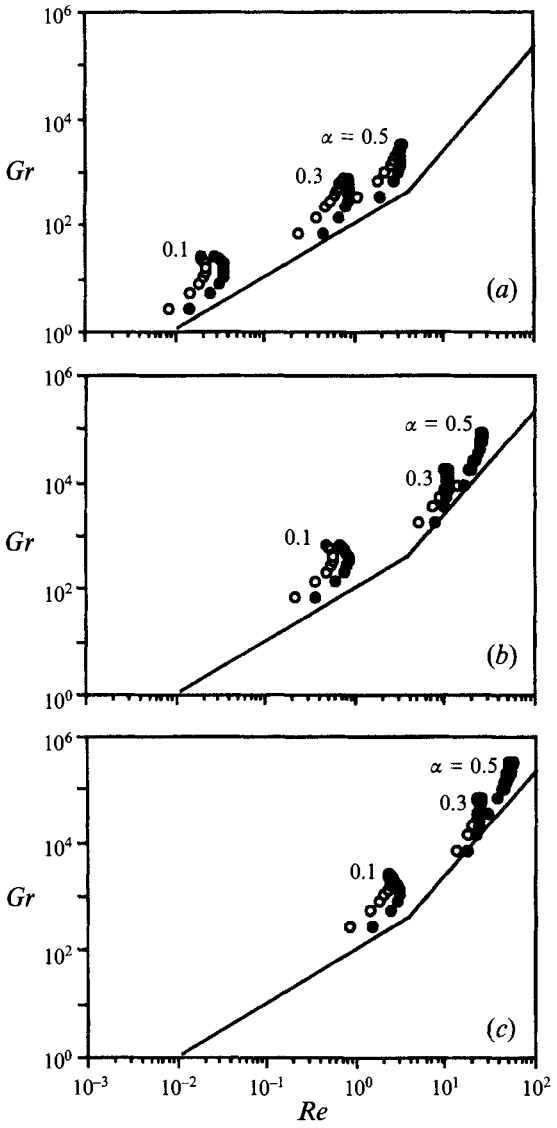

FIGURE 9. Predicted critical Reynolds numbers for elimination of the upstream (○) and downstream (●) transverse recirculations during flow of hydrogen in horizontal ducts with differentially heated lower walls. Step changes in temperature were imposed at the edges of the heated section (Case A). (*a*) $p_0 = 0.1$ atm, (*b*) $p_0 = 0.5$ atm and (*c*) $p_0 = 1.0$ atm. Other conditions: $L_s = 10$ cm, $h = 1$, 3 or 5 cm, and $T_s = 400$ to 1300 K (varied in steps of 100 K).

temperature gradients. When a more realistic boundary condition that includes conduction in the wall is used (Case B), the recirculations can be eliminated at lower *Re*. The onset of the downstream recirculation is affected more severely, because this recirculation forms near the lower wall and changes in the temperature of that wall have a significant impact on the temperature profile in the gas adjacent to it.

Computational results for Re_1 and Re_2 corresponding to different values of *Gr* are plotted in figure 9 for a hydrogen carrier gas and step changes in the temperature profile of the lower wall (Case A). The results shown in figure 9 correspond to three operating pressures and three reactor geometries. A proposed boundary, representing

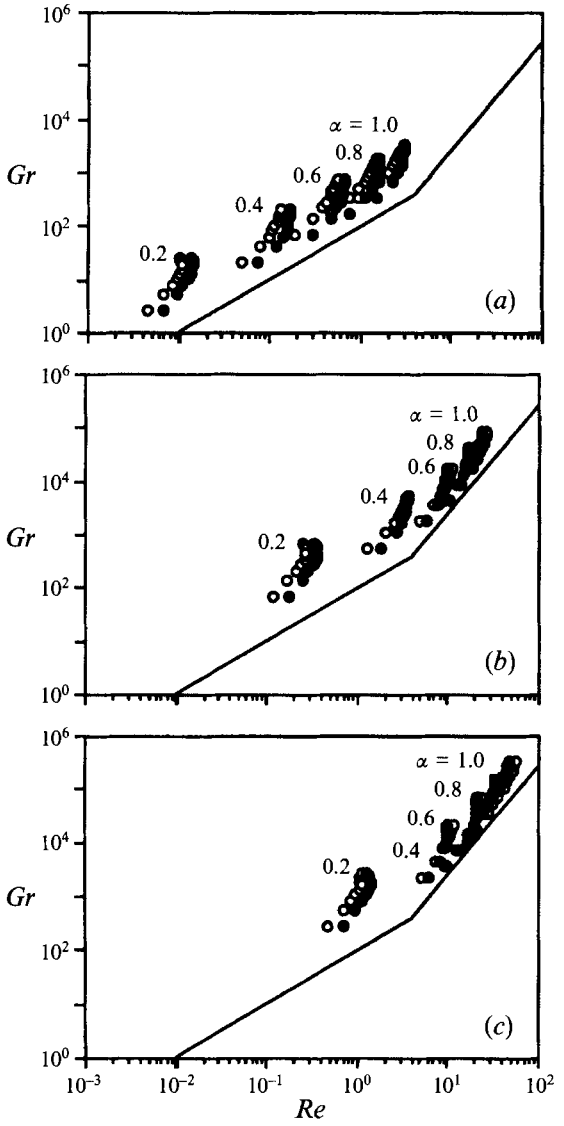

FIGURE 10. Predicted critical Reynolds numbers for elimination of the upstream (○) and downstream (●) transverse recirculations during flow of hydrogen in horizontal ducts with differentially heated lower walls. Heat conduction in the upstream and downstream parts of the lower wall has been taken into account (Case B). (*a*) $p_0 = 0.1$ atm, (*b*) $p_0 = 0.5$ atm and (*c*) $p_0 = 1.0$ atm. Other conditions: $L_s = 5$ cm, $h = 1$ to 5 cm (varied in steps of 1 cm), and $T_s = 400$ to 1300 K (varied in steps of 100 K). The data sets corresponding to $\alpha = 0.8$ and $\alpha = 1.0$ in (*c*) include additional points obtained by varying T_s from 320 to 380 K in steps of 20 K.

the transition to flows free of transverse recirculations as *Re* increases, is marked by the two straight lines. The operating conditions corresponding to the right of this boundary lead to flows free of transverse recirculations. These conditions are:

$$(Gr/Re) < 100 \quad \text{for} \quad 10^{-3} < Re \leqslant 4 \quad \text{and} \quad (Gr/Re^2) < 25 \quad \text{for} \quad 4 \leqslant Re < 100,$$

with *Gr* and *Re* computed using gas properties at the inlet conditions. The above criteria are conservative, i.e. they always guarantee absence of transverse recirculations

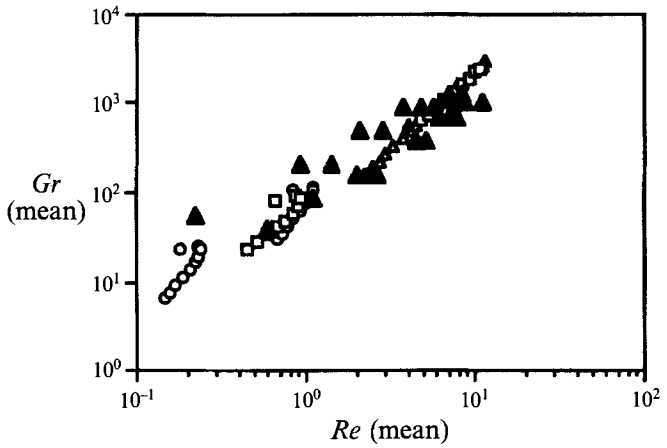

FIGURE 11. Comparison between model predictions (open symbols) and experimental observations (▲) (Visser *et al.* 1989) on the elimination of the upstream transverse recirculation during flow of hydrogen in horizontal ducts with differentially heated lower walls. The *Gr* and *Re* in this plot have been computed using gas properties evaluated at the mean temperature. The experimental points correspond to 'transitional cases' (see text) using the following operating conditions: $p_0 = 0.15 \times 10^5$–0.5×10^5 Pa, $h = 4$ cm, $T_s = 870$ and 1020 K. The predictions correspond to the following sets of operating conditions: ○, $p_0 = 0.1$ atm, $h = 3$ and 5 cm; △, $p_0 = 0.5$ atm, $h = 3$ and 5 cm; □, $p_0 = 1$ atm, $h = 1$ and 3 cm. Other conditions: $L_s = 10$ cm, and $T_s = 400$ to 1300 K in steps of 100 K.

when satisfied, and they can be used for design purposes. As is obvious from the results plotted in figure 9, the onset of transverse recirculations is not uniquely defined by a *Gr vs. Re* relation owing to the effects of temperature and pressure on gas properties.

For a more realistic case that includes a smooth temperature drop in the lower wall away from the susceptor (Case B), the proposed correlation is more conservative, as expected. Computational results for such a case are shown in figure 10 for three different pressures and five different geometries. The proposed correlation for the onset of transverse recirculations, together with the condition corresponding to the onset of longitudinal recirculations in a Boussinesq fluid (i.e. $Ra = 1708$, or $Gr = 2440$ if $Pr = 0.7$), can be very useful for predicting the structure of the flow in horizontal MOCVD reactors.

The predicted values of Re_1 for H_2 flows agree well with experimental observations of 'transitional' cases corresponding to the elimination of the upstream recirculation reported by Visser *et al.* (1989). The predictions of our model and the data of Visser *et al.* (1989) are plotted in figure 11. The data were obtained at two different susceptor temperatures, 1020 and 870 K, and at pressures ranging from 0.15×10^5 to 0.5×10^5 Pa in a reactor with a height of 4 cm. Return flows were observed for operating conditions to the left of the transitional cases and they were absent for conditions to the right of the transitional cases. The transitional cases were identified as intermediate situations for which conclusions could not be drawn by the visual inspection of the TiO_2 smoke patterns. The model predictions correspond to a range of operating conditions, which includes the experimental conditions. It should be mentioned that the values of *Gr* and *Re* plotted in figure 11 have been computed using gas properties at the mean temperatures $\frac{1}{2}(T_s + T_0)$ to allow a direct comparison between our theory and the data of Visser *et al.* (1989), because the data are reported using *Gr* and *Re* computed at the mean temperature.

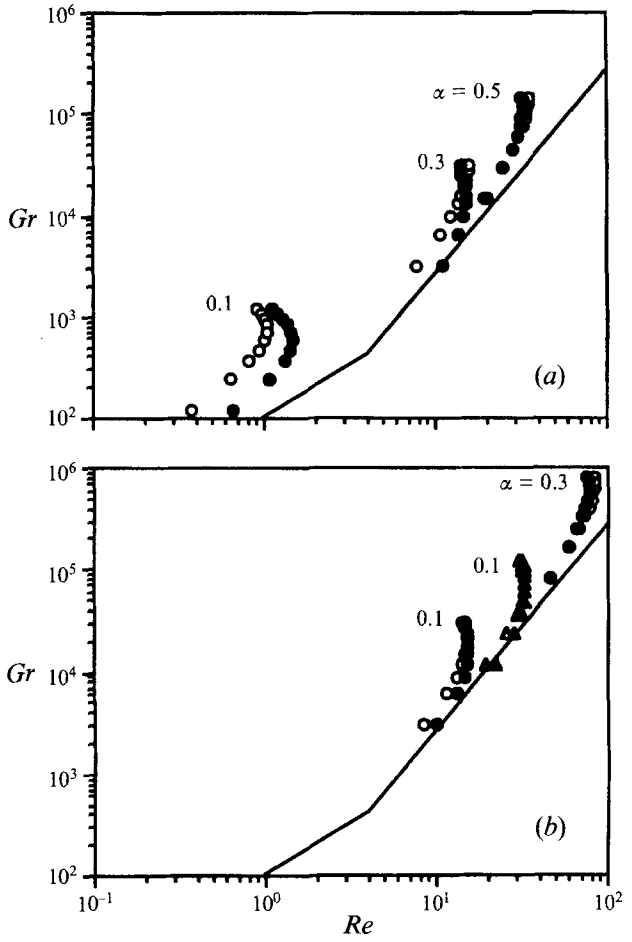

FIGURE 12. Predicted critical Reynolds numbers for elimination of the upstream (open symbols) and downstream (filled symbols) transverse recirculations during flow of nitrogen in horizontal ducts with differentially heated lower walls. Step changes in temperature were imposed at the edges of the heated section (Case A). The predictions correspond to the following sets of operating conditions: (*a*) ○, ●, $p_0 = 0.1$ atm, $h = 1$, 3 and 5 cm, 100 K. (*b*) ○, ●, $p_0 = 0.5$ atm, $h = 1$ and 3 cm; △, ▲, $p_0 = 1$ atm, $h = 1$ cm. Other conditions: $L_s = 10$ cm, and $T_s = 400$ to 1300 K in steps of 100 K.

Figure 12 shows the predicted critical *Re* for N_2 carrier gas keeping other conditions similar to the ones used in figure 9. The proposed correlation is valid in this case too and it is represented again by the two straight lines. Figure 13 compares the predicted values of Re_1 for N_2 carrier gas with experimental observations reported by Chiu & Rosenberger (1987). The observations correspond to the transition from time-dependent to steady longitudinal convection as *Re* increases. These workers used the onset of a time-periodic 'snaking' motion in the longitudinal convection rolls as an indirect way of identifying the onset of transverse recirculations near the upstream edge of the susceptor. The qualitative agreement between the predictions and the data is good, but the quantitative agreement is not very good. This is probably due to differences between the experimental set-up and the model. In the experiments, the upper wall and the isothermal upstream part of the lower wall were kept at a constant temperature of 298 K, but the inlet temperature of the gas was varied between 298.5 and 315.5 K. The temperature of the hot surface was varied between 301 and 335 K.

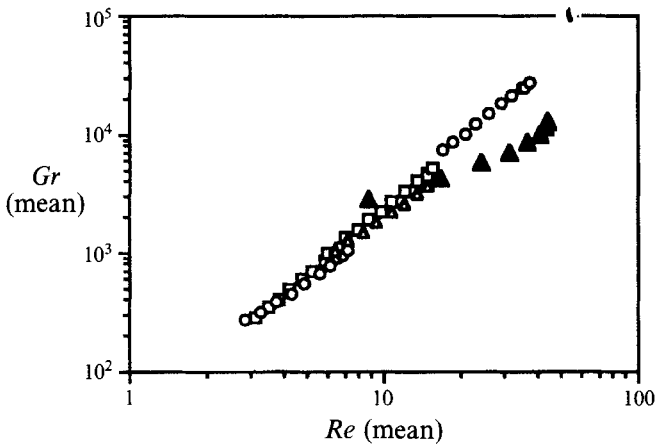

FIGURE 13. Comparison between model predictions (open symbols) and experimental observations (▲) (Chiu & Rosenberger 1987) on the elimination of the upstream transverse recirculations during flow of nitrogen in horizontal ducts with differentially heated lower walls. The experimental data correspond to transition from steady to time-dependent longitudinal convection. The *Gr* and *Re* in this plot have been computed using gas properties evaluated at the mean temperature. The observations correspond to the following operating conditions: $p_0 = 0.85$ atm, $h = 1.58$ cm, $T_s = 301$ to 335 K, wall temperature 296 K, and inlet gas temperatures from 298.5 to 315.5 K. The predictions correspond to the following sets of operating conditions: □, $p_0 = 0.1$ atm, $h = 3$ and 5 cm; ○, $p_0 = 0.5$ atm, $h = 1$ and 3 cm; △, $p_0 = 1$ atm, $h = 1$ cm. Other conditions: $L_s = 10$ cm, and $T_s = 400$ to 1300 K in steps of 100 K.

Since the flow and temperature profiles in the duct, as well as the mean values of *Re* and *Gr*, depend on these temperatures, a direct comparison between the predictions of our theory and the data is not possible. Three-dimensional effects, which cannot be captured by the present model, may have also contributed to the observed differences. It should be mentioned, however, that the quantitative agreement between theory and experiments is very good for the two data points corresponding to low experimental *Gr*, which were obtained at near isothermal upstream conditions.

Finally, simulations were performed by using the Boussinesq approximation. The results of this study were compared to the ones obtained with the full model. The conclusion was that the transverse recirculations are more persistent in a real fluid than in a Boussinesq fluid. The reason for this is that the expansion and contraction of the fluid due to heating and cooling will have a stronger effect on the inertial terms, when the density is a function of the local temperature.

7. Conclusions

A two-dimensional computational study has been performed to identify the onset of transverse buoyancy-driven recirculations during laminar flow of H_2 and N_2 in horizontal ducts with cool upper walls and lower walls consisting of a cool upstream section, a heated middle section and a cool downstream section. The motivation for this work was the need to identify optimal operating conditions in horizontal MOCVD reactors with the above geometry. Transverse recirculations were predicted both upstream and downstream of the heated section at low inlet velocities. For the range of operating conditions listed in table 1, transverse recirculations were always absent when the following criteria were satisfied:

$$(Gr/Re) < 100 \quad \text{for} \quad 10^{-3} < Re \leqslant 4 \quad \text{and} \quad (Gr/Re^2) < 25 \quad \text{for} \quad 4 \leqslant Re < 100,$$

with *Re* and *Gr* evaluated using fluid properties at the inlet conditions. This result has important implications in the optimal design of horizontal MOCVD reactors used for growing films and multi-layer structures of compound semiconductors with abrupt interfaces. The proposed correlation may also find applications in heat transfer studies in horizontal ducts. The model predictions are in good agreement with experimental observations reported in the literature.

This work was supported in part by the National Science Foundation (CTS-9010345 and CTS-9212682) and by a grant from Eastman Kodak Company. Supercomputing resources were provided by the Pittsburgh Supercomputing Center and by Cray Research, Inc., through a University Research and Development grant.

REFERENCES

BAN, V. S. 1978 Transport phenomena measurements in epitaxial reactors. *J. Electrochem. Soc.* **125**, 317–320.

CHANDRASEKHAR, S. 1981 *Hydrodynamic and Hydromagnetic Stability*. Dover.

CHINOY, P. B., AGNELLO, P. D. & GHANDHI, S. K. 1988 An experimental and theoretical study of growth in horizontal epitaxial reactors. *J. Electron. Mater.* **17**, 493–499.

CHIU, K.-C., OUAZZANI, J. & ROSENBERGER, F. 1987 Mixed convection between horizontal plates – II. fully developed flow. *Intl J. Heat Mass Transfer* **30**, 1655–1662.

CHIU, K.-C. & ROSENBERGER, F. 1987 Mixed convection between horizontal plates – I. Entrance effects. *Intl J. Heat Mass Transfer* **30**, 1645–1654.

DEARDORFF, J. W. 1965 Gravitational instability between horizontal plates with shear. *Phys. Fluids* **8**, 1027–1030.

EVANS, G. & GREIF, R. 1989 A study of traveling wave instabilities in a horizontal channel flow with applications to chemical vapor deposition. *Intl J. Heat Mass Transfer* **32**, 895–911.

EVANS, G. & GREIF, R. 1991 Unsteady three-dimensional mixed convection in a heated horizontal channel with applications to chemical vapor deposition. *Intl J. Heat Mass Transfer* **34**, 2039–2051.

EVANS, G. & GREIF, R. 1993 Thermally unstable convection with applications to chemical vapor deposition channel reactors. *Intl J. Heat Mass Transfer* **36**, 2769–2781.

EVERSTEYN, F. C., SEVERIN, P. J. W., VAN DER BREKEL, C. H. J. & PEEK, H. L. 1970 A stagnant layer model for the epitaxial growth of silicon from silane in a horizontal reactor. *J. Electrochem. Soc.* **117**, 925–931.

FIELD, R. J. 1989 Simulations of two-dimensional recirculating flow effects in horizontal MOVPE. *J. Cryst. Growth* **97**, 739–760.

FIELD, R. J. & GHANDHI, S. K. 1984 The growth of GaAs at reduced pressure in an organometallic CVD system. *J. Cryst. Growth* **69**, 581–588.

FOTIADIS, D. I., BOEKHOLT, M., JENSEN, K. F. & RICHTER, W. 1990 Flow and heat transfer in CVD reactors: Comparison of Raman temperature measurements and finite element model predictions. *J. Cryst. Growth* **100**, 577–599.

FOTIADIS, D. I. & JENSEN, K. F. 1990 Thermophoresis of solid particles in horizontal chemical vapor deposition reactors. *J. Cryst. Growth* **102**, 743–761.

GALLAGHER, A. P. & MERCER, A. McD. 1965 On the behaviour of small disturbances in plane Couette flow with a temperature gradient. *Proc. R. Soc. Lond.* A **286**, 117–128.

GILING, L. J. 1982 Gas flow patterns in horizontal epitaxial reactor cells observed by interference holography. *J. Electrochem. Soc.* **129**, 634–644.

HOLSTEIN, W. L. & FITZJOHN, J. L. 1989 Effect of buoyancy forces and reactor orientation on fluid flow and growth rate uniformity in cold-wall channel CVD reactors. *J. Cryst. Growth* **94**, 145–158.

JENSEN, K. F., EINSET, E. O. & FOTIADIS, D. I. 1991 Flow phenomena in chemical vapor deposition of thin films. *Ann. Rev. Fluid Mech.* **23**, 197–232.

LUDOWISE, M. J. 1985 Metalorganic chemical vapour deposition of III–V semiconductors. *J. Appl. Phys.* **58**, R31–R55.

MCCABE, W. L., SMITH, J. C. & HARRIOTT, P. 1985 *Unit Operations of Chemical Engineering.* McGraw-Hill.

MOFFAT, H. & JENSEN, K. F. 1986 Complex flow phenomena in MOCVD reactors I. Horizontal reactors. *J. Cryst. Growth* **77**, 108–119.

MORI, Y. 1961 Buoyancy effects in forced convection flow over a horizontal flat plate. *Trans. ASME* C: *J. Heat Transfer* **83**, 479–482.

MOUNTZIARIS, T. J., KALYANASUNDARAM, S. & INGLE, N. K. 1993 A reaction-transport model of GaAs growth by metalorganic chemical vapor deposition using trimethyl-gallium and tertiary-butyl-arsine. *J. Cryst. Growth* **131**, 283–299.

OUAZZANI, J., CHIU, K.-C. & ROSENBERGER, F. 1988 On the 2D modelling of horizontal CVD reactors and its limitations. *J. Cryst. Growth* **91**, 497–508.

OUAZZANI, J. & ROSENBERGER, F. 1990 Three-dimensional modelling of horizontal chemical vapor deposition. I. MOCVD at atmospheric pressure. *J. Cryst. Growth* **100**, 545–576.

PERRY, R. H. & CHILTON, C. H. 1973 *Chemical Engineers' Handbook* (5th edn). McGraw-Hill.

ROBERTSON, G. E., SEINFELD, J. H. & LEAL, L. G. 1973 Combined forced and free convection flow past a horizontal flat plate. *AIChE J.* **19**, 998–1008.

SPARROW, E. M. & MINKOWYCZ, W. J. 1962 Buoyancy effects on horizontal boundary-layer flow and heat transfer. *Intl J. Heat Mass Transfer* **5**, 505–511.

STOCK, L. & RICHTER, W. 1986 Vertical versus horizontal reactor: An optical study of the gas phase in an MOCVD reactor. *J. Cryst. Growth* **77**, 144–150.

STRANG, G. & FIX, G. 1973 *An Analysis of the Finite Element Method.* Prentice Hall.

VEN J. VAN DE, RUTTEN, G. J. M., RAAYMAKERS, M. J. & GILING, L. J. 1986 Gas phase depletion and flow dynamics in horizontal MOCVD reactors. *J. Cryst. Growth* **76**, 352–372.

VISSER, E. P., KLEIJN, C. R., GOVERS, C. A. M., HOOGENDOORN, C. J. & GILING, L. J. 1989 Return flows in horizontal MOCVD reactors studied with the use of TiO_2 particle injection and numerical calculations. *J. Cryst. Growth* **94**, 929–945; and errata **96**, 1989, 732–735.